Comparing Manual and Automated Digital Electrode Placement for 12-Lead ECG Using MRI-Based Torso Models

Matheus C Faesy[1], Lucas Arantes Berg[2], Lara S Rocha[1], Daniel K Almeida[1], Filipe L Namorato[1], Daniel M P Leme[1], Camille S dos Santos[3], Zhengda Ma[2], Rafael Sachetto Oliveira[4], Thaiz R Schmal[3], Thiago G S Souza[3], Abhirup Banerjee[2], Blanca Rodriguez[2], Joventino O Campos[1], Rodrigo Weber dos Santos[1]

[1] Universidade Federal de Juiz de Fora, Juiz de Fora, Brazil
[2] University of Oxford, Oxford, United Kingdom
[3] Hospital Universitário de Juiz de Fora, Juiz de Fora, Brazil
[4] Universidade Federal de São João del-Rei, São João del-Rei, Brazil

Abstract

Accurate electrode placement is crucial for reliable ECG simulation. We compare a fully automated method and a manual approach with expert input for positioning electrodes on MRI-based 3D torso meshes. Both approaches use the same heart model to generate synthetic ECGs via monodomain simulations. Pearson correlation and rRMSE indicated variable waveform similarity across leads. Sensitivity analysis revealed that limb electrodes influence multiple channels, whereas chest electrodes mostly affect their own leads. Results emphasize the importance of anatomically accurate placement in computational ECG workflows.

1. Introduction

Electrocardiography (ECG) remains a widely used diagnostic tool for assessing cardiac function, with its accuracy relying heavily on proper electrode placement on the torso surface [1]. Even small positioning errors can significantly alter ECG waveforms, potentially impacting clinical decisions.

Advances in medical imaging and segmentation have enabled personalized cardiac models from magnetic resonance imaging (MRI) or computed tomography (CT). However, mapping electrodes onto complex 3D surfaces remains challenging due to torso shape variation, conductivity differences, and user expertise [1]. To mitigate this, both automated and semi-automated electrode placement methods have been developed, often integrating image-based tools like 3D Slicer [2].

This study compares two such methods on patient-specific torso meshes: a fully automated pipeline and an expert-guided approach. Using the same heart mesh and stimulus for both, we assess how placement affects ECG morphology, highlighting trade-offs in speed, accuracy, and clinical interpretability.

2. Methods

This study investigates two different approaches for placing electrodes on 3D torso meshes, comparing their performance through ECG simulations using the MONOALG3D software. The meshes were generated after the segmentation of magnetic resonance images from a patient with dilated cardiomyopathy.

Patient Report

This study included four patients monitored at the cardiology outpatient clinic of the University Hospital at the Federal University of Juiz de Fora (UFJF). All patients underwent cardiac MRI. Table 1 summarizes the information of the cohort, where EF stands for ejection fraction.

Patient	Sex	Age (years)	Weight (kg)	EF (%)
P1	Male	71	76.4	20
P2	Female	79	54.0	21
P3	Male	71	Unknown	34
P4	Male	72	119	22

Table 1: Patient data summary

2.1. Automatic Electrode Placement

The first method consists of an automated pipeline based on [3]. The procedure uses the same MRI dataset to automatically segment both the torso and the heart. The

pipeline starts with machine learning-based torso contour extraction, where the scout MR images for each subject are first segmented using a convolutional neural network (U-Net), followed by automated post-processing and refinement through a second network [4]. Extracted contours are then used to fit a statistical shape model (SSM) of the human body, which is iteratively adjusted to match the extracted contours and form an initial torso mesh. To capture subject-specific anatomical variation, the mesh is further deformed using thin plate splines, with post-processing steps to ensure smoothness and anatomical plausibility. The locations of the ECG electrodes are identified on the mean SSM torso, and their positions are transformed with the mesh such that the resulting torso had electrodes located in equivalent locations. This fully automated workflow minimizes human intervention, ensuring high-speed processing and reproducibility across datasets.

2.2. Manual Electrode Placement

In his method only Patient 1 had an available CT scan, which enabled rib cage segmentation using TOTALSEGMENTATOR [5]. The rib cage structures, together with the sternum, were subsequently transferred to the cardiac MRI of Patient 1 using the ELASTIX registration framework [6] and the TRANSFORMIX tool. In addition, anatomical reference lines (hemiclavicular, anterior axillary, and mid-axillary) were delineated on the CT and mapped to the MRI through the same transformations. It is important to note that, even for Patient 1, all electrode placement was ultimately performed on the MRI, since the main goal of this workflow is to provide a methodology applicable to MRI-based torso segmentations.

For the remaining patients, who only had cardiac MRI, the rib cage segmentation and anatomical reference lines from Patient 1 were propagated to their MRIs using the same registration pipeline. These transferred structures provided additional anatomical landmarks, which facilitated electrode placement.

The resulting meshes and transferred anatomical guides were then loaded into a custom-developed interactive application, where clinicians manually positioned the electrodes on the torso surface. Figure 1 illustrates the interface of this tool. The application enabled navigation in the 3D environment, visualization of individual anatomical meshes, and precise placement of the 10-lead electrodes using predefined labels. Each electrode could be adjusted in 3D space through translation arrows, and its position was stored in real time.

2.3. ECG Simulation and Analysis

For both torso and electrode placements, the heart mesh generated by method in [7] was used to simulate the electrical propagation using the monodomain model through the open-source software MONOALG3D [8]. The human-based Ten Tusscher cellular model [9] was employed to describe the cellular dynamics. Cardiac tissue conductivity tensor $\boldsymbol{\sigma}$ was modeled as anisotropic, incorporating the fiber orientation and a prescribed anisotropy ratio. Temporal discretization was set at $\Delta t = 0.02\ ms$, while spatial discretization was $h = 500\ \mu m$, with $C_m = 1\ \mu F/cm^2$ and $\beta = 1400\ cm^{-1}$. An instantaneous activation was initiated simultaneously over the entire endocardial surface, and ECG signals were subsequently computed at the electrode positions.

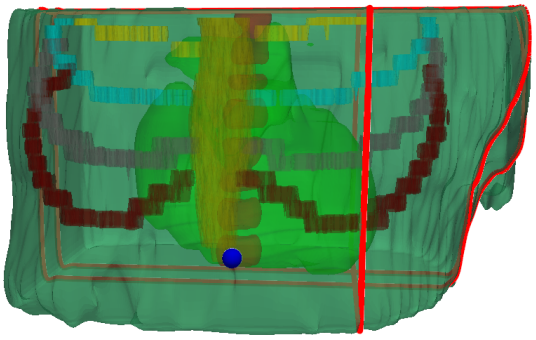

Figure 1: Interface of the custom software used for manual electrode placement.

3. Results

Figure 2 shows a 3D visualization of the torso mesh from patient 3 along with the manually and automatically placed electrodes. Each pair of corresponding electrodes is connected by a black line to indicate spatial displacement.

To quantitatively evaluate the placement differences between methods, Table 2 presents the spatial displacements between corresponding manual and automatic electrodes. For each lead and each patient, we report the differences as the Euclidean distance. All values are expressed in centimeters (cm).

Figure 3 shows the ECG waveforms from the 12 standard leads for both manual and automatic electrode configurations from patient 3. Blue lines correspond to ECGs generated with manually placed electrodes, while dashed red lines represent the signals using the automatic configuration.

Waveform comparisons reveal close agreement between manual and automatic placements in most leads, with nearly identical morphology in I, aVR, aVL, V2, V5, and V6. Noticeable discrepancies appear in leads II, III, V3, and V4, where differences in both amplitude and waveform shape can be observed. These results indicate that

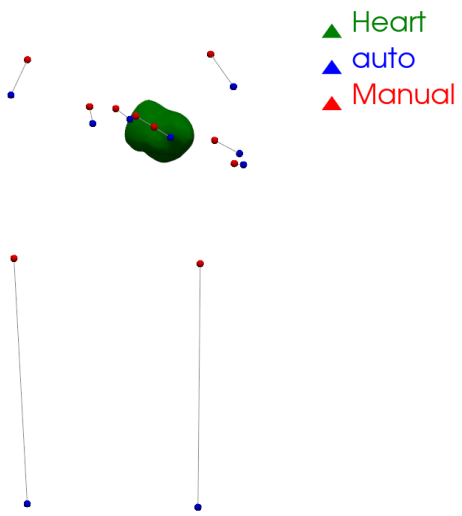

Figure 2: Three-dimensional representation of the torso and heart with manual (blue) and automatic (red) electrode placements. Black lines connect corresponding electrode pairs.

Table 2: Spatial difference between manual and automatic electrode positions (in cm).

Lead	**P1**	**P2**	**P3**	**P4**
V1	0.770	5.148	3.235	1.267
V2	1.021	5.828	3.142	1.670
V3	1.096	6.112	3.250	1.560
V4	1.344	6.310	2.725	1.279
V5	6.577	6.089	5.390	8.196
V6	4.012	6.790	1.437	4.555
LA	10.423	10.113	10.161	9.434
LL	31.714	31.613	32.613	27.082
RL	32.857	32.260	33.704	28.298
RA	10.283	8.726	9.583	9.790

while the automatic method reproduces the manual placements with high fidelity overall, the precordial leads remain particularly sensitive to small positional variations.

As shown in Table 3, Patient 1 exhibited the best overall performance, with high correlation ($r = 0.88$) and the lowest relative error (47.2%), indicating good agreement between placement strategies. In contrast, Patient 2 presented much poorer results ($r = 0.68$, rRMSE ≈87%), suggesting strong discrepancies in both waveform and amplitude. Patients 3 and 4 showed relatively high correlations ($r = 0.82$ and $r = 0.86$, respectively), but with elevated relative errors (59% and 81%).

To investigate how sensitive the final multichannel ECG is to variations in individual electrode placement, we conducted a systematic analysis: each automatic electrode was

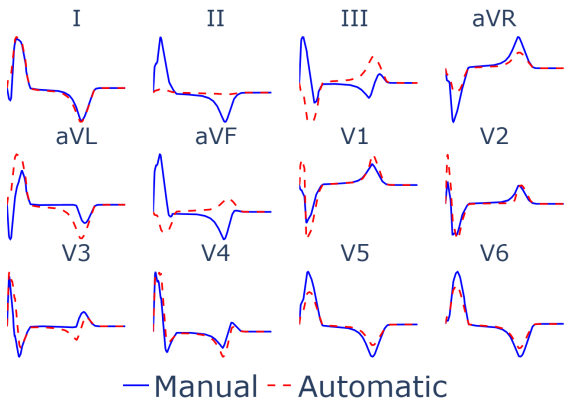

Figure 3: Comparison of 12-lead ECG signals generated from manual (blue) and automatic (dashed red) electrode placements from patient 3.

Table 3: Global results of correlation (Pearson) and relative error (rRMSE) between electrode placement strategies for each patient.

Patient	Pearson Global	rRMSE Global (%)
P1	0.8828	47.20
P2	0.6802	87.03
P3	0.8162	58.86
P4	0.8584	80.55

replaced one at a time by its corresponding manual counterpart. After each substitution, a full 12-lead ECG was computed and compared to the original fully automatic configuration. Table 4 summarizes the results of this analysis for patient 3 using the relative root mean square error (rRMSE) for each multichannel lead, expressed as a percentage. Each row in the table corresponds to the substitution of one of the ten electrodes (rows 1 to 10 represent electrodes V1–V6, LA, LL, RA, and RL respectively). Each column shows the resulting rRMSE for a specific lead in the 12-lead ECG system: leads I, II, III, aVR, aVL, aVF, and precordial leads V1–V6.

This analysis serves as a localized sensitivity test, revealing how the final 12-lead ECG is affected when a single electrode from the automatic configuration is replaced by its manual counterpart. The values in Table 4 represent the rRMSE introduced in each multichannel lead due to such substitutions.

As expected, precordial electrodes (V1–V6) exhibit strong sensitivity primarily to their corresponding leads, with errors concentrated along the diagonal of the matrix (e.g., V1 → V1 = 44%, V6 → V6 = 20%).

In contrast, limb electrodes (LA, LL, RA) exert broader influence across multiple leads. Replacing LA markedly

Table 4: rRMSE (%) for each multichannel lead after replacing one automatic electrode with the manual one for patient 3.

Lead / Electrode	I	II	III	aVR	aVL	aVF	V1	V2	V3	V4	V5	V6
V1	0	0	0	0	0	0	44	0	0	0	0	0
V2	0	0	0	0	0	0	0	45	0	0	0	0
V3	0	0	0	0	0	0	0	0	73	0	0	0
V4	0	0	0	0	0	0	0	0	0	44	0	0
V5	0	0	0	0	0	0	0	0	0	0	45	0
V6	0	0	0	0	0	0	0	0	0	0	0	20
LA	64	0	70	59	67	78	6.0	7.2	8.3	7.4	11	14
LL	0	792	79	66	38	173	6.7	8.0	9.3	8.3	13	16
RA	53	584	0	98	28	64	4.9	5.9	6.9	6.1	9.5	12

affects lead I (64%), aVL (67%), and aVF (78%), while also producing non-negligible changes in some precordial leads such as V6 (14%). Similarly, LL has a diffuse impact, particularly on II (790%), III (79%), and aVF (170%), and introduces moderate alterations in the precordials (up to 16%). RA also perturbs several limb leads (e.g., I = 53%, aVR = 98%), though its overall influence is slightly more localized compared to LA and LL.

Interestingly, V6 again emerged as the most sensitive precordial lead to variations in limb electrode positions, showing measurable deviations when LA and LL were substituted. This suggests that despite its chest location, V6 is susceptible to torso-wide field changes induced by limb electrodes.

4. Conclusion

This study compared a fully automated pipeline with respect to a semi-automatic, expert-driven approach for electrode placement on MRI-derived torso meshes, assessing their impact on simulated 12-lead ECGs. While most precordial leads showed small spatial discrepancies, limb electrodes exhibited larger deviations and stronger influence across multiple leads.

Waveform comparisons revealed that even minor spatial errors can cause significant morphological differences, particularly in V6, highlighting the clinical sensitivity of electrode positioning. Although the absence of rib cage and sternum segmentations limited definitive accuracy assessment, the results emphasize the trade-off between automation and anatomical precision, and point to the need for refined strategies in automatic electrode placement.

Acknowledgments

The authors would like to express their thanks to Minas Gerais State Research Support Foundation (FAPEMIG), “Coordenação de Aperfeiçoamento de Emprego de Nível Superior” (CAPES), “Empresa Brasileira de Serviços Hospitalares” (Ebserh), National Council for Scientific and Technological Development (CNPq), SINAPAD Santos-Dumont, and Federal University of Juiz de Fora (UFJF) for funding this work. AB is supported by the Royal Society University Research Fellowship (Grant No. URF\R1\221314).

References

[1] Garcia SL, Torres D, Martinez A, Pueyo E. Impact of electrode positioning on ecg waveforms in personalized cardiac models. Computing in Cardiology 2020;47:1–4.

[2] Pieper S, Fedorov A, Aerts HJ, Frisken S, Kapur T. 3d slicer: A platform for subject-specific image analysis and visualization. Computer Methods and Programs in Biomedicine 2022; 222:106445.

[3] Smith HJ, Rodriguez B, Sang Y, Beetz M, Choudhury R, Grau V, Banerjee A. Anatomical basis of human sex differences in ECG identified by automated torso-cardiac three-dimensional reconstruction. arXiv preprint arXiv231213976 2024;.

[4] Smith HJ, Banerjee A, Choudhury RP, Grau V. Automated torso contour extraction from clinical cardiac MR slices for 3D torso reconstruction. In 44th Annual International Conference of the IEEE Engineering in Medicine & Biology Society (EMBC). 2022; 3809–3813.

[5] Wasserthal J, Meyer M, Zimmerer D, Segeroth M, Full PM, Meine H, Maier-Hein KH. Totalsegmentator: Robust segmentation of 104 anatomical structures in ct images. Medical Image Analysis 2023;84:102680.

[6] Klein S, Staring M, Murphy K, Viergever MA, Pluim JPW. elastix: A toolbox for intensity-based medical image registration. IEEE Transactions on Medical Imaging 2010; 29(1):196–205.

[7] Banerjee A, Camps J, Zacur E, Andrews CM, Rudy Y, Choudhury RP, Rodriguez B, Grau V. A completely automated pipeline for 3d reconstruction of human heart from 2d cine magnetic resonance slices. Philosophical Transactions of the Royal Society A Mathematical Physical and Engineering Sciences 2021;379(2199):20200257.

[8] dos Santos RW, Weber GM, Rocha BM, Silva CEB, Rocha BHdP, Weber D, Corrêa AGD. Monoalg3d: A high-performance open-source code for simulating electrical activity in cardiac tissue. Computer Methods and Programs in Biomedicine 2018;164:11–18.

[9] ten Tusscher KH, Panfilov AV. Alternans and spiral breakup in a human ventricular tissue model. American Journal of Physiology Heart and Circulatory Physiology 2006; 291(3):H1088–H1100.

Address for correspondence:

Matheus Cardoso Faesy
Universidade Federal de Juiz de Fora (UFJF) Campus Universitário Rua José Lourenço Kelmer, s/n – Bairro São Pedro CEP 36036-900 – Juiz de Fora – MG, Brasil
matheusfaesy@gmail.com